

Effect of Tip Speed Ratio on the Flow Characteristics of Single-bladed Darrieus Wind Turbine

Md. Tanvir Khan, Mohammad Ilias Inam, Abdullah Al-Faruk

Department of Mechanical Engineering, Khulna University of Engineering & Technology, Khulna-9203, BANGLADESH

ABSTRACT

Wind energy is considered as one of the most realizable sources of renewable energy on the eve of fossil fuel energy depletion. Vertical axis wind turbines such as the Darrieus turbines appear to be promising for the condition of low wind speed though it has a low efficiency compared to horizontal axis turbines. The aim of this study is to investigate the flow development of a single bladed vertical axis wind turbine using CFD at different tip speed ratios. The blade is designed using the NACA 0015 profile and is operating under stalled conditions. Two dimensional simulations are performed using ANSYS Fluent 16.2, employing the realizable k-epsilon turbulence model and scalable wall function. Simple pressure-based solver is selected along with the second order implicit transient formulation. The CFD results under dynamic cases are presented and the resulting aerodynamic forces are evaluated. The turbine is observed to generate both positive and negative power at certain azimuthal angles. The pressure contours, velocity profiles as well as the velocity streamlines are illustrated and the powers and the power coefficients are calculated. Results show that force as well as the power is proportional to the tip speed ratio and at every case net average power is positive. Moreover, force as well as power varies periodically with the azimuthal angles. Finally, the average power and power coefficient are calculated after the turbine has come to steady state condition—that increase with the tip speed ratios.

Keywords: Darrieus wind turbine, power coefficient, pressure coefficient, tip speed ratio, vortex.

1. Introduction

The focus on Renewable Energy Resources has increased significantly in the recent years in the wake of growing environmental pollution, rising energy demand and depleting fossil fuel resources. Different renewable energy sources include solar, biomass, geothermal, hydroelectric, wind etc. Among these the Eolic energy source (wind power) has proved to be a cheaper alternative energy resource and hence extensive research efforts have been put to improve the technology of electricity generation through it [1]. The world has enormous potential of wind energy that can be utilized for electricity generation [2]. Wind power is now world's one of the fastest growing energy resources [2]. Although the vertical axis wind turbine (VAWT) was the first ever wind turbine to be used for harnessing wind energy [3], researchers of the modern era lost interest in it for the initial perception that VAWT cannot be used for large scale electricity generation. Horizontal axis wind turbine (HAWT) remained the focus of all wind energy related research activity for last few decades. However, research work on VAWT continued in parallel at a relatively smaller scale. Scientists and Engineers developed various wind turbine configurations and utilized different approaches for their analysis. Optimum conditions for the working of VAWTs were determined. Some of these techniques and configurations of researchers on vertical axis wind turbines are reviewed in this paper. A closer look on the concepts leads towards the fact that VAWTs are suitable for electricity generation in the conditions where traditional HAWTs are unable to give reasonable efficiencies such as high wind velocities [3], and turbulent wind flows [3]. Moreover, vertical axis wind

turbines are convenient for power generation in the built environment like urban, suburban or remote areas [3]. Another major advantage is that VAWTs are Omni-directional, accepting wind from any direction without any yawing mechanism [3]. VAWT has a number of promising features which if exploited properly can make it a better alternative to fulfill the world's energy demand [4]. Although currently large scale VAWTs are not economically attractive, they offer energy solutions for remote places away from the main distribution lines and places where large wind farms cannot be installed for environmental concerns and small-scale dispersed generation units are preferred [4]. That is why mass production of VAWTs has recently been started as small scale wind power generating units [5].

Two types of VAWTs, namely, Savonius wind turbine (SWT) and Darrieus wind turbine (DWT) are available. Among them DWT is more suitable for power production for high rotating speed [6]. Darrieus is a lift type wind turbine of which the blades are of airfoil shaped. A huge amount of research has been done on Darrieus wind turbine and still continuing. Castelli and Benini [7] presented the effect of blade thickness on the operation of a straight-bladed vertical axis wind turbine (SVAWT) in a 2D, time accurate, numerical simulations. Castelli and Ardizzone [8] performed a numerical analysis on a small DWT to make a systematic comparison with wind tunnel experimental data. Result proved that the best near-blade grid element dimension can be determined through statistical analysis of some indicators, such as the Y^+ parameter, to maximize the accuracy of the numerical prediction of rotor performance while maintaining a reasonable computational effort. Ferreira [9, 10] investigated the

effect of the dynamic stall in a 2D single-bladed SVAWT, which reports the influence of the turbulence model in the simulation of the vertical structures spread from the blade itself. Vassberg [11] tried to improve the efficiency of a VAWT by applying the emerging CFD capabilities through the simulation of the dynamic motion of a turbine blade including the parametric study of turbine solidity, turbine tip speeds and a variation of NACA 0015 section. Owing to the occurrence of most structural failures of wind turbines in the blade root section, a 3D analytical model of HAWT, blades constructed of NACA 0015, was proposed by Chazly [12] using bending triangular plate finite elements to compute the deflection, stresses, and eigenvalues in the rotor blades. Compendium of the proposition is—maximum stresses occurred at the root of the blades in the span wise direction and in addition to saving material weight—a tapered blade—diminished the stresses obtained. Moreover, the twisting blade leads to enhance stiffness and decrease stresses. A CFD model was presented by Castelli and Englaro [13] for the evaluation of energy performance and aerodynamic forces acting on a SVAWT of Darrieus type. In which the basic principles that are currently applied to Blade Element-Momentum (BE-M) theory for rotor performance prediction are transferred to the CFD code, that allow the correlation between flow geometric characteristics (such as blade angles of attack) and dynamic quantities (such as rotor torque and blade tangential and normal forces). Energy performance and aerodynamic forces acting on a helical SVAWT was evaluated by Castelli and Benini [14] depending on the blades inclined to the horizontal plane to generate a phase shift angle of 0°, 30°, 60°, 90° and 120° between lower and upper blade sections, for a rotor with an aspect ratio of 1.5.

The tip speed ratio is the relationship between rotor blade velocity and relative wind velocity which is defined by, $\lambda = \frac{\omega R}{U}$, where, ω = Rotor rotational speed in radian/second, R = Rotor radius in meter, U = Wind velocity. It is the foremost design parameter around which all other optimum rotor and blades dimensions are calculated. Higher tip speeds result in higher noise levels and require stronger blades due to large centrifugal forces [15]. The tip speed ratio is a very important aspect; therefore, efficiency, torque, mechanical stress, aerodynamics and noise should be considered in selecting the appropriate tip speed. Besides, it has been found to produce efficient conversion of the wind's kinetic energy into electrical power [15]. This paper aims to investigate the flow development of a single bladed vertical axis Darrieus wind turbine using CFD methods under different tip speed ratios. The turbine blade was constructed of NACA 0015 airfoil shape. Two dimensional simulations were performed using ANSYS Fluent software 16.2 version, employing the Realizable K-epsilon turbulence model [16] with scalable wall function. The CFD results from the dynamic case were presented and the resulting

aerodynamic forces were evaluated. Also, The Power coefficients for different tip speed ratios were calculated.

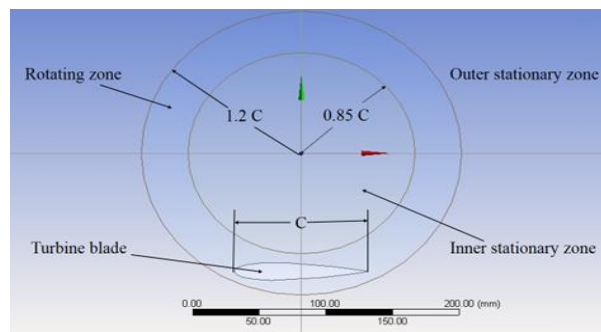
2. Numerical model development

ANSYS FLUENT provides the opportunity to solve both

steady state and transient flow analyses with a variety of turbulence modeling. Continuity equation and Navier Stokes equation are solved in all CFD analysis, and in compressive flow or heat transfer cases. A numerical model was developed for this simulation, where the governing equations were employed to describe the flow over the turbine. Continuity and momentum equations were included in the models the model as the model neglects heat transfer. All the governing equations are described in the literature [16].

3. Computational set up

The computational domain was constructed of two different zones, namely, stationary zone and rotating zone including the turbine blade [17]. The rotating zone, generated bi-directionally from the blade surface resulting in an annulus shaped zone, rotates at a



predefined angular velocity as shown in Fig.1. The square shaped domain dimension is 50C by 50C, based on chord length (C) and the center of the rotating zone is placed at the middle of the square, which is also chosen by Mohamed [16]. Before finalize the domain, different domain sizes were taken and the domain independence test was done.

Fig.1 Domain of numerical analysis

Different sizes of unstructured mesh were employed in this analysis, combining element size of 0.003 mm near the blade for precisely analyzing the flow characteristics and 0.008 mm further from the blade. 20 inflation layers were used with 5 mm thickness in the vicinity of the blade surface to better resolve the boundary layer as illustrated in Fig.2. The selected node and element numbers were 1232362 and 2459030, respectively, after executing grid independence test. The combined grid was chosen instead of single grid to reduce the complexity of the mesh generation. The similar technique was employed in the literature [17, 18, and 19] and good agreements with the measurements were shown. The stationary and rotating zones were linked via the sliding interface boundary condition.

Velocity inlet and pressure outlet boundary conditions were used at the upstream and downstream section, respectively, and symmetry condition was used at the other two sides to reduce the computational effort as done

by Castelli [20, 21]. The blade was placed in the rotating zone that can rotate with the rotating zone of the same angular velocity between the stationary zones. No slip wall is set as the boundary condition on the blade surface.

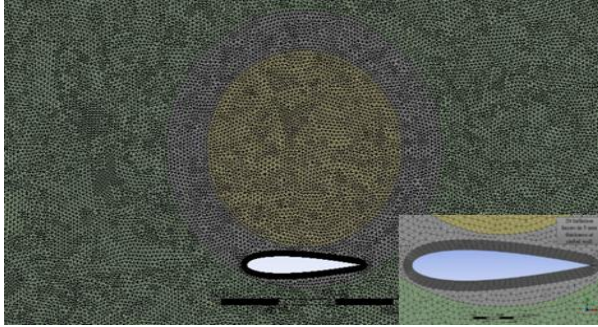


Fig.2 Generated mesh around the domain

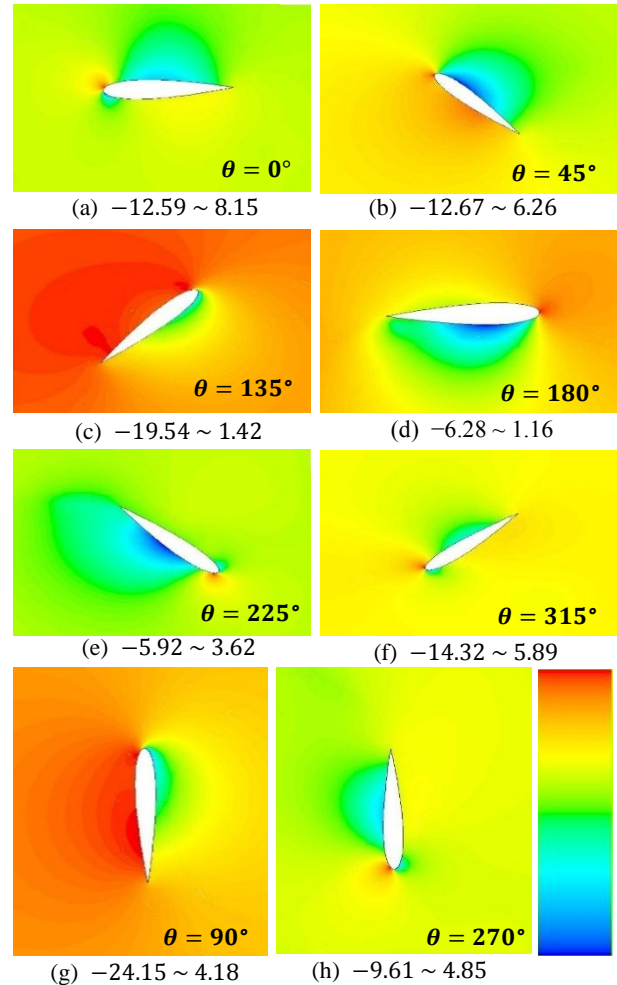
To capture the flow phenomena around the blade precisely, as minimal as 0.005 time step size was used after time independence verification. The turbine blade was set with an initial clockwise rotation and the air was allowed to flow around the turbine blade at a known velocity (2.5 m/s). Due to wind velocity, a net torque was developed for the combined effect of the air kinetic energy and the blade rotation. The normal and tangential force as well as the power had been calculated from the developed lift and drag force on the blade at each azimuthal position. Realizable $k-\epsilon$ turbulence model, referred by Mohammed [16], was used for rotating zones due to improved performance in flow circulation, strong pressure gradients, flow separation, and non-reliance on an assumed relationship between the Reynolds stress tensor and the strain rate tensor. Simple pressure based solver was selected along with second order implicit transient formulation. All solution variables were solved via the second order upwind discretization scheme that is also followed by Bangga [17]. Scalable wall function was used and $Y^+ \geq 11.126$ was ensured for the analysis.

4. CFD results

The simulations were carried out for 10 blade revolutions and the last three revolutions were extracted and averaged which is also done by Bangga [17]. Flow characteristics around the blade are observed and different types of vortex, generated for dynamic stall and the blade vortex interaction, are analyzed. The tangential (F_T) force, normal (F_N) force and the average power coefficient for different tip speed ratios had been calculated from the simulation data.

4.1 Flow field analysis of DWT

Flow characteristics such as pressure coefficient contour, velocity contour and streamline has been determined after every 45° interval of azimuthal angle (θ) in the analysis. Pressure coefficient is a dimensionless number that describes the relative pressure throughout a flow field and is defined by, $C_p = \frac{P - P_\infty}{1/2 \rho_\infty V_\infty^2}$ [22]. It is a vital factor for wind turbine aerodynamics which causes a significant change in the lift and drag as well as the power generation. It is observed from **Fig.3(a)** pressure at the upper surface of the blade is less than the lower surface at the beginning of the turbine rotation when $\theta = 0^\circ$. Air strikes at the turbine tip and



maximum pressure occurs there which is called the stagnation point. Velocity at the upper surface is higher than the lower surface as shown in **Fig.4(a)**. Theoretically, no lift force is generated at

Fig.3 Contour of pressure coefficient with different azimuthal angle θ at 2.5 m/s wind velocity and tip speed ratio 2. The minimum and maximum values of the color legend are mentioned below the figure.

this position of the blade. Flow separates from the trailing edge and a negative (anticlockwise) vortex is visible at the lower surface **Fig.5 (a)**. The more the turbine rotates the more flow separation starts from the leading edge and Stall formation occur after the flow

separation. Maximum pressure occurs at the lower surface at $\theta = 45^\circ$ where the air strikes **Fig.3(b)**. Pressure at upper surface is lower than the lower surface. Velocity near the tip is very high from where the flow separates. Velocity at the upper surface is greater than the lower surface according to the Bernoulli equations as illustrated in **Fig.4(b)**. A positive (clockwise) trailing edge vortex (TEV) forms at the lower surface of the blade **Fig.5(b)**. High pressure drag occurs at the upstream of the blade at $\theta = 90^\circ$ due to high air kinetic energy as shown in **Fig.3(g)**. Separation occurs from both the leading and the trailing edge of the blade and maximum velocity occurs at the leading edge of the blade **Fig.4(g)**. Positive vortex occurs at the middle of the upstream of the blade and at the downstream near the blade as observed in **Fig.5 (g)**. Flow separations occur both from the leading edge and the trailing edge at $\theta = 135^\circ$. A positive TEV is visible

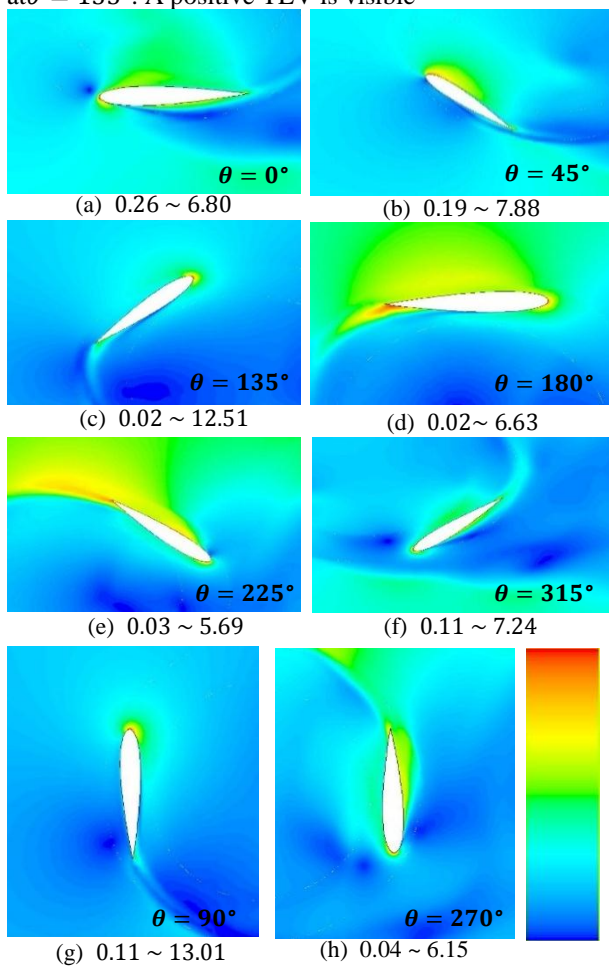


Fig.4 Contour of velocity profile with different azimuthal angle θ at 2.5 m/s wind velocity and tip speed ratio 2. The minimum and maximum values of the color legend are mentioned below the figure.

at this position which tends to separate **Fig.5(c)**. Pressure is higher at the upstream than the downstream of the blade and maximum velocity occurs at the leading-edge **Fig.3(c)**. Another negative vortex (LEV) formation starts at the leading edge of the blade due to the

dynamic stall (DS). Low pressure occurs below the blade and maximum pressure is at the leading edge of the blade at $\theta = 180^\circ$ **Fig.3(d)**. Velocity at the trailing edge is maximum and higher velocity occurs at the upper surface than the lower surface of the blade **Fig.4(d)**. Different types of vortex are visible at this position of blade. Positive LEV and TEV and another negative vortex are visible at a little distance from the blade as shown in **Fig.5(d)**. The lower pressure zone does not separate from the lower surface of the blade at $\theta = 225^\circ$ **Fig.3 (e)** due to the high speed of the turbine blade. Velocity at the trailing edge is higher than another zone as illustrated in **Fig.4(e)**. Different negative vortices are visible near the blade's leading edge and trailing edge due to the dynamic stall and blade vortex interaction **Fig.5(e)**. Pressure at the leading edge is maximum at $\theta = 270^\circ$ **Fig.3 (h)** and velocity at the downstream is higher than the upstream **Fig.4(h)**. Flow separation occurs from both the leading and the trailing

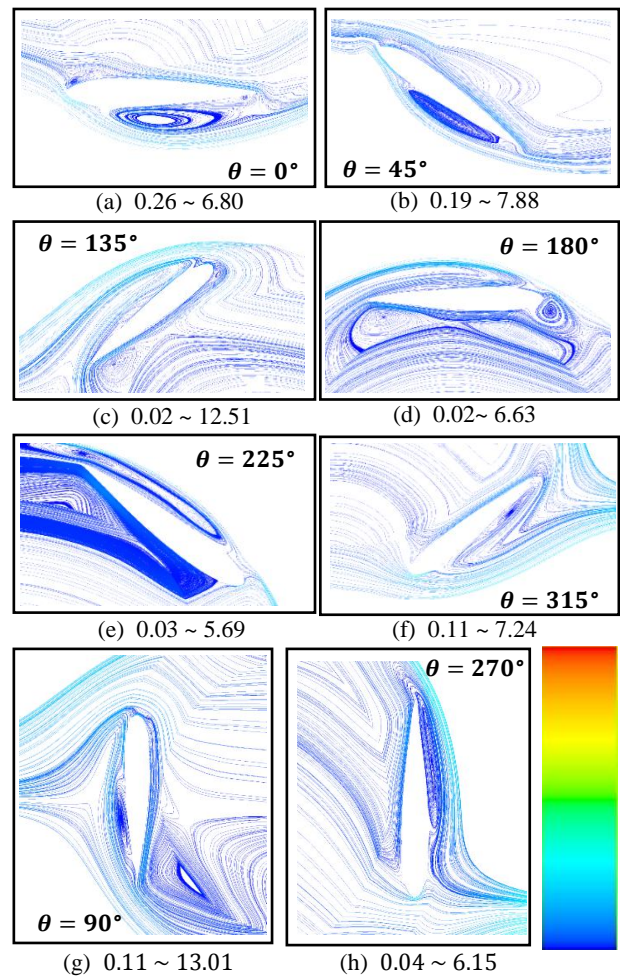


Fig.5 Contour of stream line with different azimuthal angle θ at 2.5 m/s wind velocity and tip speed ratio 2. The minimum and maximum values of the color legend are mentioned below the figure.

edge and a small negative TEV is formed and tends to separate from the blade **Fig.5(h)**. Pressure at lower

surface of the blade is greater than the upper surface and maximum Pressure occur at the blade tip at $\theta = 315^\circ$ as shown in Fig.3 (f). The previously formed TEV becomes smaller. Flow separates from both the leading edge and the trailing edge and reattachment occur at a little distance from the blade Fig.5(f). In the presence of laminar-turbulent transition, flow may reattach in such a way that, initially laminar boundary flow may separate because of an adverse pressure gradient. Then the flow becomes strongly unstable and hence turbulent. Hence, it reattaches further downstream because of the stronger resistance of turbulent boundary-layer flow against separation. After the cycle complete the flow phenomena repeats as the turbine come to a steady state.

4.2 Tangential (F_T) and Normal (F_N) force

The tangential and normal forces vary periodically after the 7th revolution of the rotor blade in the simulation. Both the forces are proportional to the tip speed ratios. Tangential force occurs due to the wind flow tangent to the blade surface whether normal force occur perpendicular to the blade. Lift and drag forces were calculated from the lift (C_L) and drag (C_D) coefficient and then tangential and normal forces were calculated from the lift and drag forces.

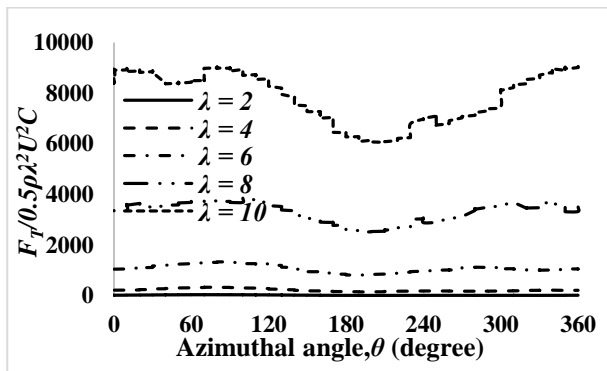


Fig.6 Variation of Tangential Force with Azimuthal Angle for different Tip Speed Ratios

It is observed from Fig.6 that, tangential force in the total cycle is positive. F_T increase from $\theta = 0^\circ$ to $\theta = 90^\circ$ and then decreases for the generation of a vortex (TEV) at the trailing edge. As the TEV stays till $\theta = 200^\circ$ the tangential force tends to decrease. When the TEV separates, force starts increasing and continues for the rest of the cycle. It is discerned that the tangential force decreases due to the TEV.

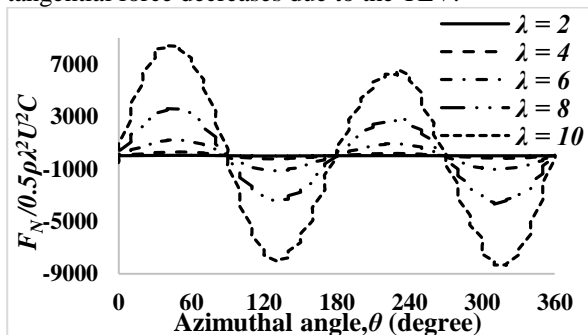


Fig.7 Variation of Normal Force with Azimuthal Angle for different Tip Speed Ratios

The normal force around the blade is zero when the turbine is at $\theta = 0^\circ$ as illustrated in Fig.7. However, F_N starts increasing with the increment of the azimuthal angle and gain a maximum value at $\theta = 45^\circ$. Then F_N tends to decrease till $\theta = 135^\circ$ and from $\theta = 90^\circ$ the value of the force become negative. However, F_N starts increasing at $\theta = 135^\circ$ up to $\theta = 225^\circ$ and from $\theta = 180^\circ$ the values become positive. Again the force decrease till $\theta = 315^\circ$ and at $\theta = 270^\circ$ the value becomes negative. Finally F_N increase for the rest of the cycle. For the variation of azimuthal angle with the flow direction the normal forces show these natures. It is observed that F_N is positive at the 1st and the 3rd quarter and the rest of the cycle F_N is negative.

4.3 Angle of attack (α)

The angle of attack varies periodically with the azimuthal angle (θ) by, $\alpha = \tan^{-1} \left[\frac{\sin \theta}{(\lambda + \cos \theta)} \right]$. The magnitude of α change as the sine curve as illustrated in Fig.8.

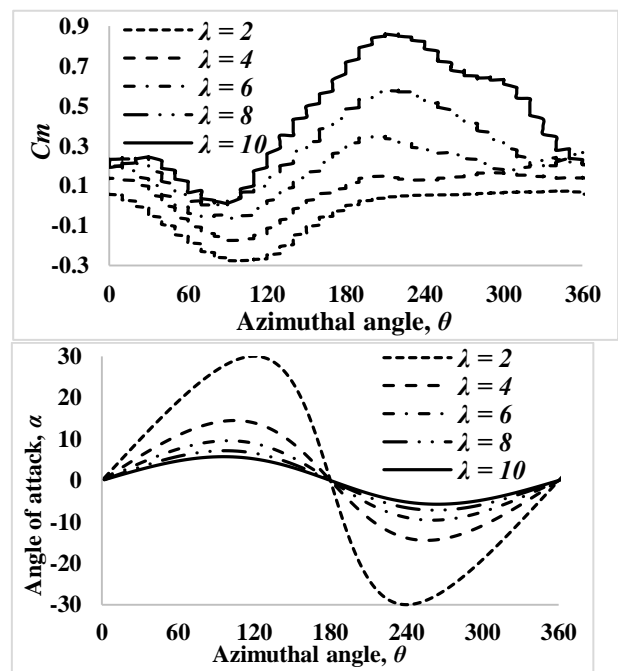


Fig.8 Variation of angle of attack with azimuthal angle at different tip speed ratio

4.4 Torque coefficient (C_m)

Torque/moment coefficient (C_m) is varying periodically with the azimuthal angle (θ). Torque coefficient is decreasing up to $\theta = 90^\circ$ but after that C_m increasing

and attain a maximum value between $\theta = 180^\circ$ and $\theta = 240^\circ$ as shown in **Fig.9**.

Fig.9 Variation of moment coefficient with azimuthal angle at different tip speed ratio

4.5 Power coefficient

Power coefficient is the ratio of the generated output power (P) to the theoretical input power (P_{in}). As the turbine rotates clockwise direction the negative tangential force (F_T) generate the positive power which can be defined by, $P = -\omega R F_t$ [17]. The theoretical input power is $P_{in} = \frac{1}{2} \rho A V^3$, where A is the swept area, V is the air velocity and ρ is air density. The variation of power coefficient is similar to the variation of F_T with azimuthal angle. The values of power coefficients are 2.95, 17.42, 53.14, 128.59, and 267.37 for the tip speed ratios which indicate that average power coefficient is gradually increasing with the tip speed ratios. Variation of average power with the tip speed ratio follows 2nd order polynomial curve as shown in **Fig.10**.

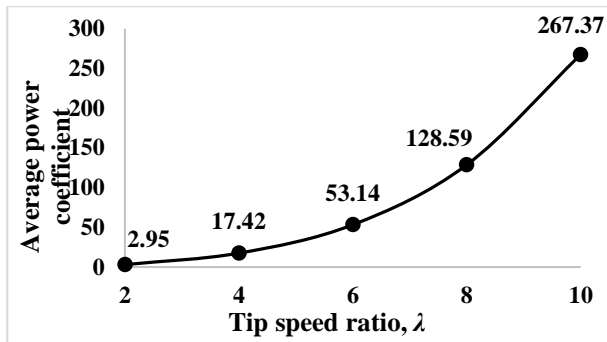


Fig.10 Average power coefficient at different tip speed ratios

5. Conclusions

Numerical analysis has been carried out to study a single-bladed Darrieus wind turbine at different tip speed ratios (2, 4, 6, 8, 10). The studied turbine blade was constructed of NACA 0015 airfoil profile and operating under the dynamic stalled condition. Investigation of the flow characteristics around the bladed surface were highlighted as the main focus of the paper. The tangential and normal force and the average power coefficient had been calculated. Moreover, the torque coefficient around the blade was determined. It is observed that positive and negative vortices generate around the blade surface as a consequence of dynamic stall. As a result, pressure varies considerably that affect the tangential forces as well as power production. The forces and the power coefficients, varying positively and negatively with the azimuthal angle, are periodic and proportional to the tip speed ratios. The average power coefficients at the steady state are positive which indicate that the turbine can produce net positive power.

NOMENCLATURE

λ : tip speed ratio

C_p : pressure coefficient
 F_T : tangential force, N
 F_N : normal force, N
 C_m : torque coefficient

REFERENCES

- [1] Batista, N. C., Melício, R., Mendes, V. M., Figueiredo, J., & Reis, A. H. (2013, April). Darrieus Wind Turbine Performance Prediction: Computational Modeling. In *Doctoral Conference on Computing, Electrical and Industrial Systems* (pp. 382-391). Springer, Berlin, Heidelberg.
- [2] Ponta, F. L., Seminara, J. J., & Otero, A. D. (2007). On the aerodynamics of variable-geometry oval-trajectory Darrieus wind turbines. *Renewable Energy*, 32(1), 35-56.
- [3] Chaichana, T., & Chaitep, S. (2010). Wind power potential and characteristic analysis of Chiang Mai, Thailand. *Journal of mechanical science and technology*, 24(7), 1475-1479.
- [4] Bishop, J. D., & Amaratunga, G. A. (2008). Evaluation of small wind turbines in distributed arrangement as sustainable wind energy option for Barbados. *Energy Conversion and Management*, 49(6), 1652-1661.
- [5] Islam, M., Fartaj, A., & Ting, D. S. K. (2004). Current utilization and future prospects of emerging renewable energy applications in Canada. *Renewable and Sustainable Energy Reviews*, 8(6), 493-519.
- [6] Bhutta, M. M. A., Hayat, N., Farooq, A. U., Ali, Z., Jamil, S. R., & Hussain, Z. (2012). Vertical axis wind turbine—A review of various configurations and design techniques. *Renewable and Sustainable Energy Reviews*, 16(4), 1926-1939.
- [7] Castelli, M. R., & Benini, E. (2011, September). Effect of blade thickness on Darrieus Vertical-Axis Wind turbine performance. In *CSSim 2011, 2nd International Conference on Computer Modelling and Simulation* (pp. 5-7).
- [8] Castelli, M. R., Ardizzon, G., Battisti, L., Benini, E., & Pavesi, G. (2010, January). Modeling strategy and numerical validation for a Darrieus vertical axis micro-wind turbine. In *ASME 2010 International Mechanical Engineering Congress and Exposition* (pp. 409-418). American Society of Mechanical Engineers.
- [9] Ferreira, C. S., Bijl, H., Van Bussel, G., & Van Kuik, G. (2007). Simulating dynamic stall in a 2D VAWT: modeling strategy, verification and validation with particle image velocimetry data. In *Journal of physics: conference series* (Vol. 75, No. 1, p. 012023). IOP Publishing.
- [10] Simao Ferreira, C., Van Bussel, G., Van Kuik, G., & Scarano, F. (2007, January). 2D PIV visualization of dynamic stall on a vertical axis wind turbine. In *45th AIAA Aerospace Sciences Meeting and Exhibit* (p. 1366).
- [11] Vassberg, J., Gopinath, A., & Jameson, A. (2005). Revisiting the vertical-axis wind-turbine design using advanced computational fluid dynamics. In *43rd AIAA Aerospace Sciences Meeting and Exhibit* (p. 47).
- [12] El Chazly, N. M. (1993). Static and dynamic analysis of wind turbine blades using the finite element method. *International journal for numerical methods in engineering*, 36(16), 2791-2804.
- [13] Castelli, M. R., Englaro, A., & Benini, E. (2011). The Darrieus wind turbine: Proposal for a new performance prediction model based on CFD. *Energy*, 36(8), 4919-4934.
- [14] Castelli, M. R., & Benini, E. (2012). Effect of blade inclination angle on a Darrieus wind turbine. *Journal of turbomachinery*, 134(3), 031016.
- [15] Wind Turbine Tip Speed Ratio | REUK.co.uk". www.reuk.co.uk. Retrieved 14 May 2017

- [16] Mohamed, M. H., Ali, A. M., & Hafiz, A. A. (2015). CFD analysis for H-rotor Darrieus turbine as a low speed wind energy converter. *Engineering Science and Technology, an International Journal*, 18(1), 1-13.
- [17] Bangga, G., Hutomo, G., Wiranegara, R., & Sasongko, H. (2017). Numerical study on a single bladed vertical axis wind turbine under dynamic stall. *Journal of Mechanical Science and Technology*, 31(1), 261-267.
- [18] Qin, N., Howell, R., Durrani, N., Hamada, K., & Smith, T. (2011). Unsteady flow simulation and dynamic stall behaviour of vertical axis wind turbine blades. *Wind Engineering*, 35(4), 511-527.
- [19] Hutomo, G., Bangga, G., & Sasongko, H. (2016). CFD studies of the dynamic stall characteristics on a rotating airfoil. *Applied Mechanics and Materials*, 836, 109-114.
- [20] Castelli, M. R., Englaro, A., & Benini, E. (2011). The Darrieus wind turbine: Proposal for a new performance prediction model based on CFD. *Energy*, 36(8), 4919-4934.
- [21] Castelli, M. R., Dal Monte, A., Quaresimin, M., & Benini, E. (2013). Numerical evaluation of aerodynamic and inertial contributions to Darrieus wind turbine blade deformation. *Renewable Energy*, 51, 101-112.
- [22] Anderson Jr, J. D. (2010). *Fundamentals of aerodynamics*. Tata McGraw-Hill Education.